Journal of Photochemistry and Photobiology A: Chemistry 221 (2011) 47–57

Contents lists available at ScienceDirect

Journal of Photochemistry and Photobiology A: Chemistry

journal homepage: www.elsevier.com/locate/jphotochem

Phenanthrenyl-indole as a fluorescent probe for peptides and lipid membranes

Bruno F. Hermenegildo[a], Goreti Pereira[b], Ana S. Abreu[a,b], Elisabete M.S. Castanheira[a,*], Paula M.T. Ferreira[b], Maria-João R.P. Queiroz[b]

[a] Centro de Física (CFUM), Universidade do Minho, Campus de Gualtar, 4710-057 Braga, Portugal
[b] Centro de Química (CQ-UM), Universidade do Minho, Campus de Gualtar, 4710-057 Braga, Portugal

ARTICLE INFO

Article history:
Received 30 December 2010
Received in revised form 12 April 2011
Accepted 21 April 2011
Available online 29 April 2011

Keywords:
Phenanthrenyl-indole
RGD-peptide
Fluorescence
Lipid membranes

ABSTRACT

A 3-(Phenanthren-9-yl)-1*H*-indole-2-carboxylic acid (**2**) obtained from the cleavage of the methyl ester of the methyl 3-(phenanthren-9-yl)-1*H*-indole-2-carboxylate (**1**) was inserted into a peptide containing the RGD sequence. The GGRGDG peptide sequence was prepared by solid phase synthesis and coupled to compound (**2**), using diisopropylcarbodiimide (DIC) and 1-hydroxybenzotriazole (HOBt) in DMF. The peptide (**3**) labelled with the phenanthrenylindole moiety was obtained in 31% yield.

The photophysical properties of the phenanthrenyl-indole derivatives were studied in several solvents of different polarity. Compounds **1** and **2** have reasonably high fluorescence quantum yields (between 27% and 85%) in non-protic solvents, the methyl phenanthrenyl-indole-2-carboxylate **1** being the more fluorescent compound. The fluorescence emission of both compounds is sensitive to solvent, indicating that they are good candidates for fluorescent probes. Fluorescence emission measurements of the labelled peptide in solution showed a strong decrease of Φ_F value caused by the attachment of the Gly-Gly-Arg-Gly-Asp-Gly chain.

The phenanthrenyl-indoles **1** and **2** and the labelled peptide **3** were incorporated in liposomes of dipalmitoyl phosphatidylcholine (DPPC) and dipalmitoyl phosphatidylglycerol (DPPG) and mixtures of both lipids. Steady-state anisotropy measurements showed that compounds **1** and **2** are located inside the lipid bilayers and are able to report the transition between the gel and liquid-crystalline phases. The RGD labelled peptide locates mainly in the outer part of the vesicle interface. These results indicate that the phenanthrenyl-indole moiety may be used as a fluorescent probe for peptides and lipid membranes.

1. Introduction

Fluorescence spectroscopy is widely used to study proteins and peptides, with the vast majority of studies making use of the naturally occurring fluorophores, tyrosine and tryptophan. However, there is considerable interest in the incorporation of novel fluorophores, because they can offer site specific probes and, in many cases, can be chosen to allow selective excitation and detection [1,2]. Fluorescent peptides form a new generation of analytical tools for visualizing intracellular processes and molecular interactions at the level of single cells [3,4]. The sequence arginine-glycine-aspartic acid (RGD) (Fig. 1) is found in many extracellular matrix proteins and is responsible for their interaction with a class of cell receptors known as integrins. These receptors are involved in the regulation of cellular proliferation and apoptosis. In particularly the integrin $\alpha_v\beta_3$ is over-expressed in some tumour cells and has been implicated in essential processes in the growth of solid tumours and in the development of metastases [5–9].

In our laboratories we have been interested in the synthesis of new heterocyclic compounds that could be used as fluorescent probes for biological systems [10]. One of the strategies developed for the synthesis of these compounds involves the Suzuki–Miyaura cross-coupling of brominated dehydroamino acids with aryl boronic acids followed by a metal assisted C–N intramolecular cyclisation [11]. Using this methodology we were able to prepare a variety of indole derivatives and also to study their photophysical properties [10]. Among these compounds, the methyl 3-(phenanthren-9-yl)-1*H*-indole-2-carboxylate was prepared and showed to be a good candidate to be used as a fluorescence probe for biological systems [10c]. Continuing this work, it was decided to link this compound to a peptide containing the arginine-glycine-aspartic acid (RGD) sequence.

The absorption and emission properties of the methyl 3-(phenanthren-9-yl)-1*H*-indole-2-carboxylate, 3-(phenanthren-9-yl)-1*H*-indole-2-carboxylic acid and of the labelled peptide were studied in both homogeneous solution and incorporated in lipid

Abbreviations: DPPC, dipalmitoyl phosphatidylcholine; DPPG, dipalmitoyl phosphatidylglycerol; PC, phosphatidylcholine; PG, phosphatidylglycerol; G, glycine; R, arginine; D, aspartic acid.

* Corresponding author. Tel.: +351 253 604321; fax: +351 253 604061.
E-mail addresses: ecoutinho@fisica.uminho.pt, emsccoutinho@gmail.com (E.M.S. Castanheira).

1010-6030/$ – see front matter © 2011 Elsevier B.V. All rights reserved.
doi:10.1016/j.jphotochem.2011.04.022

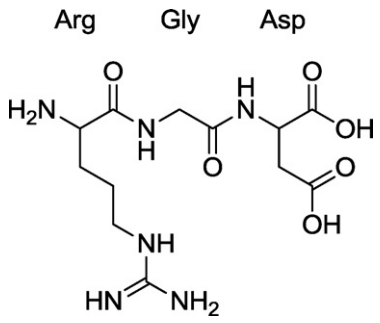

Fig. 1. Tripeptide Arg-Gly-Asp.

membranes of dipalmitoyl phosphatidylcholine and/or dipalmitoyl phosphatidylglycerol which are the main components of biological membranes.

2. Experimental

2.1. Materials and methods

Melting points (°C) were determined in a Gallenkamp apparatus and are uncorrected. ^{1}H and ^{13}C NMR spectra were recorded on a Bruker Avance III at 400 and 100.6 MHz, respectively. ^{1}H–^{1}H spin–spin decoupling and DEPT θ 45° were used. HMQC and HMBC were used to attribute some signals. Chemical shifts are given in ppm and coupling constants in Hz. HRMS data were recorded by the mass spectrometry service of the University of Vigo, Spain.

All the solutions were prepared using spectroscopic grade solvents and ultrapure water (Milli-Q grade). 1,2-Dipalmitoyl-*sn*-glycero-3-phosphocholine (DPPC) and 1,2-dipalmitoyl-*sn*-glycero-3-[phospho-*rac*-(1-glycerol)] (sodium salt) (DPPG) were purchased from Sigma–Aldrich (lipid structures are shown below).

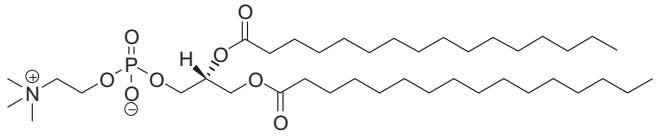

DPPC

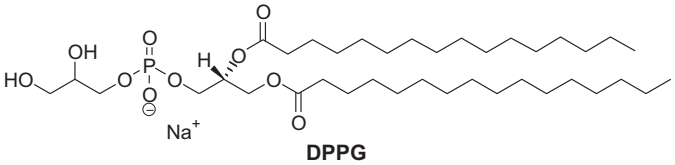

DPPG

For phospholipid vesicles preparation, the injection method was used [10b,12–14]. Defined volumes of stock solutions of lipid (50 mM in ethanol for DPPC and 13.4 mM in tetrahydrofuran for DPPG) and compounds **1** and **2** (0.197 mM for **1**, and 0.195 mM for **2**) were injected together at 60 °C, well above the melting transition temperature of DPPC (*ca.* 41 °C) [15] and DPPG (39.6 °C) [16], under vigorous stirring, to an aqueous buffer solution (10 mM Tris–HCl, pH = 7.2) also at 60 °C. In all cases, the final lipid concentration was 1 mM, with compounds/lipid molar ratio of 1:500.

2.2. Spectroscopic measurements

Absorption spectra were recorded in a Shimadzu UV-3101PC UV–Vis–NIR spectrophotometer. Fluorescence measurements were performed using a Fluorolog 3 spectrofluorimeter, equipped with double monochromators in both excitation and emission, Glan-Thompson polarizers and a temperature controlled cuvette holder. Fluorescence spectra were corrected for the instrumental response of the system.

For fluorescence quantum yield determination, the solutions were previously bubbled for 40 min with ultrapure nitrogen. The fluorescence quantum yields (Φ_s) were determined using the standard method (Eq. (1)) [17,18]. 9,10-Diphenylanthracene in ethanol ($\Phi_r = 0.95$ [19]) was used as reference.

$$\Phi_s = \frac{A_r F_s n_s^2}{A_s F_r n_r^2} \Phi_r \quad (1)$$

where A is the absorbance at the excitation wavelength, F is the integrated emission area and n is the refraction index of the solvents used. Subscripts refer to the reference (r) or sample (s) compound. The absorbance value at excitation wavelength was always less than 0.1, in order to avoid inner filter effects.

Solvatochromic shifts were described by the Lippert–Mataga equation (2), which relates the energy difference between absorption and emission maxima to the orientation polarizability [20,21]

$$\overline{\nu}_{abs} - \overline{\nu}_{fl} = \frac{1}{4\pi\varepsilon_0} \frac{2\Delta\mu^2}{hcR^3} \Delta f + const \quad (2)$$

where $\overline{\nu}_{abs}$ is the wavenumber of maximum absorption, $\overline{\nu}_{fl}$ is the wavenumber of maximum emission, $\Delta\mu = \mu_e - \mu_g$ is the difference in the dipole moment of solute molecule between excited (μ_e) and ground (μ_g) states, R is the cavity radius (considering the fluorophore a point dipole at the center of a spherical cavity immersed in the homogeneous solvent), and Δf is the orientation polarizability given by (Eq. (3)):

$$\Delta f = \frac{\varepsilon - 1}{2\varepsilon + 1} - \frac{n^2 - 1}{2n^2 + 1} \quad (3)$$

where ε is the static dielectric constant and n the refractive index of the solvent.

The steady-state fluorescence anisotropy, r, is calculated by

$$r = \frac{I_{VV} - GI_{VH}}{I_{VV} + 2GI_{VH}} \quad (4)$$

where I_{VV} and I_{VH} are the intensities of the emission spectra obtained with vertical and horizontal polarization, respectively (for vertically polarized excitation light), and $G = I_{HV}/I_{HH}$ is the instrument correction factor, where I_{HV} and I_{HH} are the emission intensities obtained with vertical and horizontal polarization (for horizontally polarized excitation light).

2.3. Synthesis

*Synthesis of the methyl 3-(phenanthren-9-yl)-1H-indole-2-carboxylate (**1**)*: The synthesis of this compound was described elsewhere [10c].

*Synthesis of 3-(phenanthren-9-yl)-1H-indole-2-carboxylic acid (**2**)*: A solution of NaOH 1 M (3 equiv.) was added to a solution of **1** (0.6260 mmol; 0.220 g) in methanol (0.1 mol dm^{-3}) and the mixture was heated at reflux. When all the reagent had been consumed (4 h) the methanol was removed and the solution was acidified to pH = 1–2 with HCl (5 mol dm^{-3}). Filtration of the solid formed afforded compound **2** (0.200 g, 94%); m.p. 205–206 °C. ^{1}H NMR (400 MHz, $CDCl_3$): 7.09 (t, J = 6.8 Hz, 1H, ArH), 7.29 (d, J = 8.4 Hz, 1H, ArH), 7.36–7.45 (m, 3H, ArH), 7.60–7.72 (m, 4H, ArH), 7.79 (s, 1H, ArH), 7.87 (d, J = 8.4 Hz, 1H, ArH), 8.77 (t, J = 7.6 Hz, 2H, ArH), 9.18 (br s, 1H, NH) ppm. ^{13}C NMR (100.6 MHz, $CDCl_3$): 111.91 (CH), 121.04 (CH), 122.20 (CH), 122.59 (CH), 122.73 (CH), 123.48 (C), 123.68 (C), 126.39 (CH), 126.46 (CH), 126.47 (CH), 126.68 (CH), 126.73 (CH), 126.84 (CH), 128.73 (CH), 129.06 (C), 129.16 (CH), 129.80 (C), 130.33 (C), 130.35 (C), 131.52 (C), 131.69 (C),

136.12 (C), 165.94 (C=O) ppm. HRMS (micrOTOF) [M+H]: calcd. for $C_{23}H_{15}NNaO_2$ 360.09950; found 360.09938.

*Synthesis of peptide (**3**)*: The GGRGDG peptide was prepared by solid phase synthesis using a Fmoc strategy. Fmoc-Gly-OH (1.2 equiv.) and diisopropylethylamine (DIPEA) (4 equiv. relative to the amino acid) in dry dichloromethane (DCM) were added to the 2-chlorotrityl chloride resin (0.5 g). The mixture was left stirring for 2 h. At end of this time, the resin was washed with a mixture of DCM/MeOH/DIPEA (17:2:1) (3× 20 mL), DMF (2× 20 mL) and DCM (2× 20 mL). The resin was dried in vacuum and the determination of the first residue attachment made by cleaving Fmoc with DBU and measuring the solution concentration of dibenzofulvene by UV spectroscopy. The loading amount was 0.58 mol g^{-1}. After cleavage of the Fmoc group with a solution of piperidine in DMF, couplings were carried out using an excess of the Fmoc-amino acid (4 equiv., 1.20 mmol) with diisopropylcarbodiimide (DIC) and 1-hydroxybenzotriazole (HOBt) in DMF. Compound **2** (0.58 mmol, 195.6 mg) was coupled to the last amino acid using a similar strategy. The peptide labelled with the phenanthrenylindole was cleaved from the resin using a mixture of acetic acid/1,1,1-trifluoroethanol/DCM (2:2:6). The protecting groups were removed with TFA to give peptide **3** as a yellow solid (150.5 mg, 31%). ^{1}H NMR (400 MHz, DMSO-d_6): 11.97 (s, 1H, NH), 8.91 (t, J = 9.6 Hz, 1H, ArH), 8.64 (br s, 1H, NH), 8.30–8.20 (m, 4H, ArH + NH), 8.14–7.87 (m, 5H, ArH + NH), 7.75–7.64 (m, 4H, ArH + NH), 7.59–7.46 (m, 3H, ArH + NH), 7.29–6.94 (m, 6H, ArH + NH_3^+), 4.59–4.56 (m, 1H, α-CH Asp), 4.28–4.22 (m, 1H, α-CH Arg), 3.84–3.61 (m, 8H, CH_2 Gly), 3.08–2.98 (m, 2H, δ-CH Arg), 2.67–2.52 (m, 2H, β-CH_2 Asp), 1.71–1.37 (m, 4H, β + γ CH_2 Arg). ^{13}C NMR (400 MHz, DMSO-d_6): 24.77 (CH_2), 28.84 (CH_2), 36.36 (CH_2), 40.43 (CH_2), 40.35 (CH_2), 41.98 (CH_2), 42.08 (CH_2), 49.52 (CH), 52.43 (CH), 42.40 (CH_2), 112.50 (CH), 115.93 (C), 115.99 (C), 120.14 (CH), 120.33 (CH), 122.83 (CH), 123.21 (CH), 124.16 (CH), 126.50 (CH), 126.55 (CH), 126.66 (CH), 126.72 (CH), 126.91 (CH), 126.96 (CH), 128.70 (CH), 129.32 (CH), 129.80 (C), 130.09 (C), 130.29 (C), 131.35 (C), 131.43 (C), 135.51 (C), 166.53 (C=N), 168.52 (C=O), 168.68 (C=O), 168.77 (C=O), 170.92 (C=O), 170.98 (C=O), 171.04 (C=O), 171.75 (C=O), 171.84 (C=O). HRMS (micrOTOF) [M+H]: calcd. for $C_{41}H_{45}N_{10}O_{10}$ 837.33146; found 837.33039.

3. Results and discussion

3.1. Synthesis

The methyl 3-(phenanthren-9-yl)-1*H*-indole-2-carboxylate (**1**) [10c] was prepared from a β-bromodehydrophenylalanine and 9-phenanthracenylboronic acid by a Suzuki–Miyaura cross-coupling followed by a Pd/Cu assisted C–N intramolecular cyclisation developed in our research group [10]. This compound was inserted into a peptide containing the RGD sequence after cleavage of the methyl ester (Scheme 1). Thus, compound **1** was treated with sodium hydroxide in methanol to afford the corresponding carboxylic acid (**2**) in a 94% yield. Compound **2** was conjugated with the hexapeptide glycine-glycine-arginine-glycine-aspartic acid-glycine (GGRGDG) synthesized by standard solid phase peptide synthesis (SPPS) using a fluorenylmethoxycarbonyl (Fmoc) protocol and a 2-chlorotrityl chloride resin. For side-chain protection the 2,2,4,6,7-pentamethyl dihydrobenzofuran-5-sulfonyl (Pbf) group for arginine and the *tert*-butyl (^{t}Bu) group for aspartic acid were used. Coupling reactions were performed with diisopropylcarbodiimide (DIC) and 1-hydroxybenzotriazole (HOBt). Compound **2** was coupled in solid phase using the same conditions. After cleavage from the resin and removal of the protecting groups, the labelled peptide **3** was obtained in 31% yield.

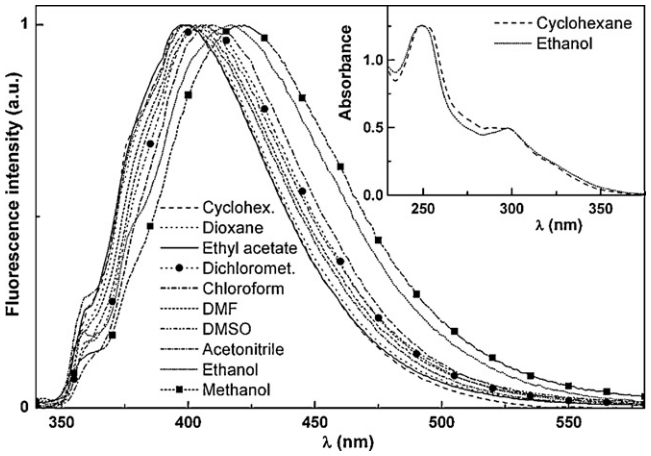

Fig. 2. Normalized fluorescence spectra of 2×10^{-6} M solutions of compound **1** in several solvents (λ_{exc} = 325 nm). Inset: absorption spectrum of 2×10^{-5} M solutions of **1** in cyclohexane and ethanol, as examples.

3.2. Fluorescence of compounds *1* and *2* in several solvents

The absorption and emission properties of compounds **1** and **2** were studied in ten solvents of different polarity. The maximum absorption (λ_{abs}) and emission wavelengths (λ_{em}), molar absorption coefficients (ε) and fluorescence quantum yields (Φ_F) are presented in Table 1. The normalized fluorescence spectra of the phenanthrenyl-indoles **1** and **2** are shown in Figs. 2 and 3, respectively. Examples of absorption spectra are shown as insets.

In indole and its derivatives the near-ultraviolet absorption is generally attributed to two strongly overlapping $\pi \rightarrow \pi^*$ transitions [22–24], with an average ε value for non substituted indole of 5550 M^{-1} cm^{-1}, which also justifies its relatively high fluorescence quantum yield [25]. Compound **1** presents high ε values ($\varepsilon > 1.2 \times 10^4$ M^{-1} cm^{-1}) at the lowest energy maximum in all solvents studied, while for compound **2** the ε values are significantly lower ($\varepsilon \geq 3.9 \times 10^3$ M^{-1} cm^{-1}) (Table 1). Many carbonyl compounds have a low-lying $n \rightarrow \pi^*$ state, exhibiting low fluorescence quantum yields. As a carbonyl group is present in both compounds, the $\pi \rightarrow \pi^*$ and $n \rightarrow \pi^*$ electronic transitions can be nearby in energy, resulting in state-mixing [26]. The high values of the molar absorption coefficient for compound **1** can indicate a predominance of the $\pi \rightarrow \pi^*$ character, the latter being less pronounced for compound **2**.

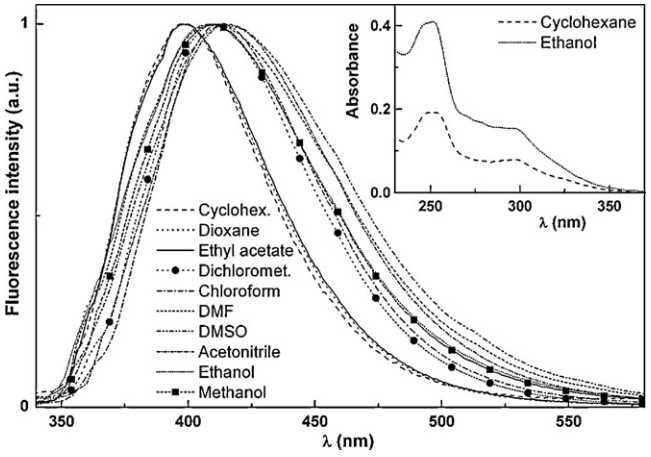

Fig. 3. Normalized fluorescence spectra of 2×10^{-6} M solutions of compound **2** in several solvents (λ_{exc} = 325 nm). Inset: absorption spectrum of 2×10^{-5} M solutions of **2** in cyclohexane and ethanol, as examples.

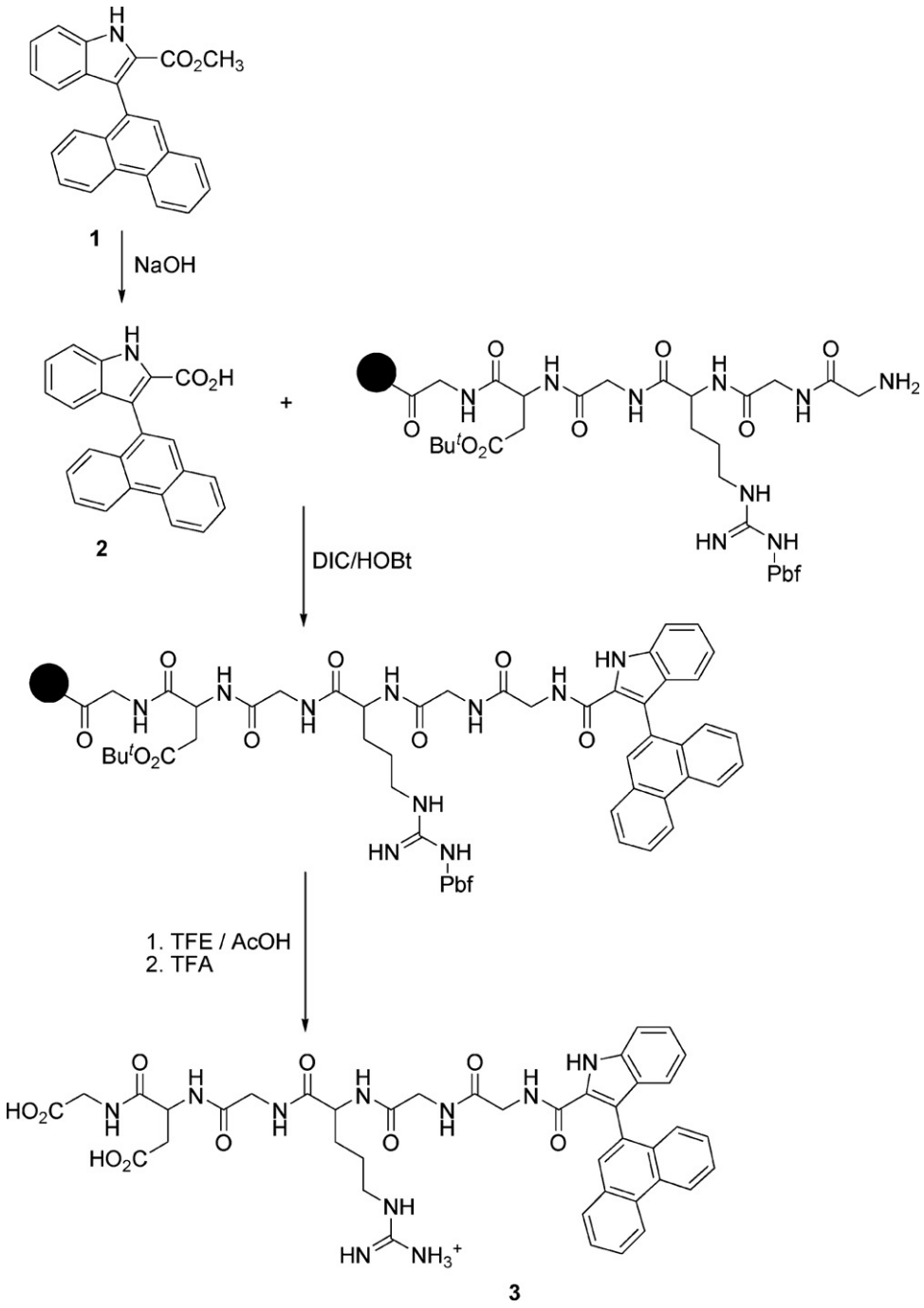

Scheme 1. Synthesis of compound **2** and peptide **3**.

For both compounds, significant red shifts are observed for emission in polar solvents, that are larger for compound **2**, if alcohols are not considered. In the absorption spectra, the red shifts are negligible (Table 1), indicating that solvent relaxation after photoexcitation plays an important role. In polar solvents, a clear band enlargement in emission is also observed (Figs. 2 and 3), which is usually related to an intramolecular charge transfer (ICT) mechanism and/or to specific solvent effects [20]. This behaviour was already observed in other indole derivatives previously synthesized by us, namely the methyl 3-arylindole-2-carboxylates [27], the 1-heteroaryl-3*H*-benzothieno or benzofuroindole-2-carboxylates [28], and several heteroaryl and heteroannulated indoles [29].

The Lippert–Mataga plots for compounds **1**–**2**, shown in Fig. 4, are reasonably linear in non-protic solvents, chloroform, alcohols and water exhibiting large positive deviations for the phenanthrenyl-indole **1**. This behaviour can be due to specific solute–solvent interactions by hydrogen bonds. Both compounds have the capability of hydrogen bonding formation through the NH group (donor) and the carbonyl group (acceptor). The formation of hydrogen bonds between chloroform and proton acceptors is known since a long time [31]. However, the Lippert–Mataga plot for compound **2** shows a small negative deviation for alcohols. One possible explanation for this fact could be the formation, in the ground state, of a hydrogen bond between the H atom of the carboxylic group and alcohols that becomes weaker in the excited state. The same behaviour does not occur in water, that exhibits a usual large positive deviation for both compounds (Fig. 4). The generally larger solvatochromic shifts for compound **2** point to a

Table 1
Maximum absorption (λ_{abs}) and emission wavelengths (λ_{em}), molar absorption coefficients (ε) and fluorescence quantum yields (Φ_F) for compounds **1** and **2** in several solvents.

Solvent	λ_{abs} (nm) ($\varepsilon/10^4$ M^{-1} cm^{-1})		λ_{em} (nm)		Φ_F[a]	
	1	**2**	**1**	**2**	**1**	**2**
Cyclohexane	298 (2.47) 249 (6.27) 226 (5.14)	297 (0.39) 252 (0.96) 226 (0.76)	399	397	0.70	0.28
Dioxane	298 (2.85) 249 (6.97) 226 (6.23)	298 (0.65) 249 (1.55) 227 (1.35)	400	400	0.49	0.48
Ethyl acetate	297 (2.68)[b]	297 (0.65)[b]	400	403	0.85	0.33
Dichloromethane	298 (1.22) 249 (2.94) 226 (2.82)	298 (0.51) 250 (1.22) 228 (1.03)	404	410	0.80	0.34
N,*N*-Dimethylformamide	299 (2.71)[b]	298 (0.57)[b]	405	412	0.63	0.42
Dimethylsulfoxide	300 (2.61)[b]	299 (0.64)[b]	407	415	0.84	0.62
Acetonitrile	297 (2.25) 248 (5.88) 226 (4.64)	297 (0.56) 248 (1.39) 225 (1.17)	403	414	0.55	0.30
Chloroform	299 (2.58)[b]	299 (0.69)[b]	410	412	0.85	0.27
Ethanol	298 (2.47) 249 (6.26) 227 (4.84)	298 (0.77) 248 (2.05) 225 (1.85)	417	410	0.57	0.11
Methanol	297 (2.55) 248 (6.30) 226 (5.10)	298 (0.63) 247 (1.73) 225 (1.78)	422	412	0.52	0.07
Water	297 (0.42) 249 (0.75) 226 (0.80)	298 (0.71) 251 (3.12) 225 (1.70)	426	431	0.02	0.09

[a] Relative to 9,10-diphenylanthracene in ethanol (Φ_F = 0.95 at 25 °C [19]). Error about 10%.
[b] *Solvents cut-off*: dimethylsulfoxide: 270 nm; *N*,*N*-dimethylformamide: 275 nm; ethyl acetate: 265 nm; chloroform: 250 nm.

higher ICT character of the excited state for this compound, due to the presence of a carboxylic acid group.

From *ab initio* molecular quantum chemistry calculations, obtained with Gaussian 09 software [32] and use of a 6-311+G(dp) basis set at the TD-SCF DFT (B3LYP) level of theory [33] in gas phase, the cavity radius (R) and the ground state dipole moment (μ_g) were determined for the two compounds (Table 2). The optimized geometry of the ground state of phenanthrenyl-indoles **1** and **2** shows that the indole-2-carboxylate/carboxylic acid moiety is roughly perpendicular to the phenanthrene rings, while in the lower excited state a distortion occurs, with the approximation of the phenanthrenyl and indole moieties (Fig. 5). The direction of the calculated dipole moments in the ground and excited states are also indicated.

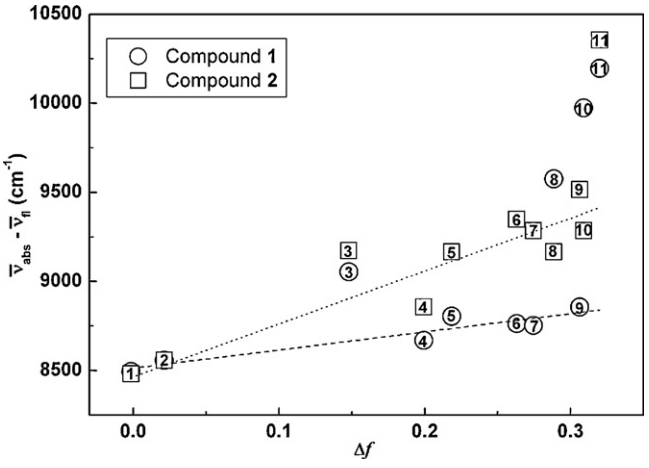

Fig. 4. Lippert–Mataga plots for compounds **1** and **2**. Solvents: 1—cyclohexane; 2—dioxane; 3—chloroform; 4—ethyl acetate; 5—dichloromethane; 6—dimethylsulfoxide; 7—*N*,*N*-dimethylformamide; 8—ethanol; 9—acetonitrile; 10—methanol; 11—water (values of ε and n were obtained from Ref. [30]).

The values of excited state dipole moments, estimated from the Lippert–Mataga plots and from molecular quantum mechanical calculations, are presented in Table 2. The values obtained from the calculations are slightly lower than the ones estimated from the Lippert–Mataga plots. Nevertheless, the μ_e values and the change in direction of the dipole moment (Fig. 5) point to the presence of a significant charge transfer mechanism in the excited state, especially for the compound with the carboxylic group.

Fig. 6 displays the representation of HOMO and LUMO molecular orbitals for the two compounds, obtained with the calculated optimized geometries for ground and lowest excited singlet state. The HOMO molecular orbital is mainly located in the phenanthrenyl moiety, with a small contribution of the indole-2-carboxylate/carboxilic group, more significant for compound **1**. The HOMO–LUMO transition (for both geometries) of these phenanthrenyl-indoles shows an almost complete charge transfer from the phenanthrene rings to the indole-2-carboxylate/carboxylic moiety. This confirms the CT character of the excited state, more pronounced for compound **2**.

When in the excited state geometry, it is observed in LUMO molecular orbital of both compounds an additional electron density between the oxygen of the carbonyl group and a nearby double bond of the phenanthrenyl moiety. This occurs as, due to the geometrical distortion, the distance between this oxygen atom and the C–C bond in the phenanthrenyl ring decreases from 3.7 Å to 2.7 Å.

Fig. 7 shows the representation of the energy level diagram with the transition energies of both compounds. The mentioned additional electron density is probably responsible for the significant decrease in LUMO energy upon geometrical relaxation of the excited state. These results predict a large Stokes' shift that is, in fact, observed in the experimental data. The calculated absorption and emission transition energies are at lower energies than the ones experimentally observed. This can be due to solvent effects not accounted on the *ab initio* calculations as these were performed in the gas phase.

Table 2
Cavity radius (R) and ground state dipole moments (μ_g), obtained from theoretical calculations, and excited state dipole moments (μ_e) calculated from the Lippert–Mataga plots and from quantum mechanical calculations.

Compound	Cavity radius, R (Å)	Ground state dipole moment, μ_g (D)	Excited state dipole moment, μ_e (D), from Lippert–Mataga plots	Excited state dipole moment, μ_e (D), from theoretical calculations
1	5.7	2.81	7.2	6.9
2	5.6	2.53	10.0	8.1

Both compounds present reasonable to high fluorescence quantum yields in almost all solvents, compound **1** attaining 85% in some solvents (Table 1). A notable reduction of Φ_F is observed for compound **2** in alcohols, probably caused by an increase of singlet → triplet intersystem crossing efficiency through H-bond interaction.

The generally high fluorescence quantum yields and solvent sensitive emission of compounds **1** and **2** make them good candidates as fluorescence probes for biological membranes and proteins, as they can be excited without simultaneous excitation of tryptophan and other aromatic amino acids (tyrosine and phenylalanine) of proteins, which absorb light at λ < 300 nm [20].

3.3. *Fluorescence of peptide **3** in homogeneous solution*

Fig. 8 shows the absorption (inset) and fluorescence spectra of the peptide **3** in ethanol and aqueous medium (pH = 7). A red shift (*ca.* 15 nm) and band enlargement is observed in aqueous media. Fluorescence quantum yields are presented in Table 3. It can be observed a strong fluorescence quenching of compound **1** caused

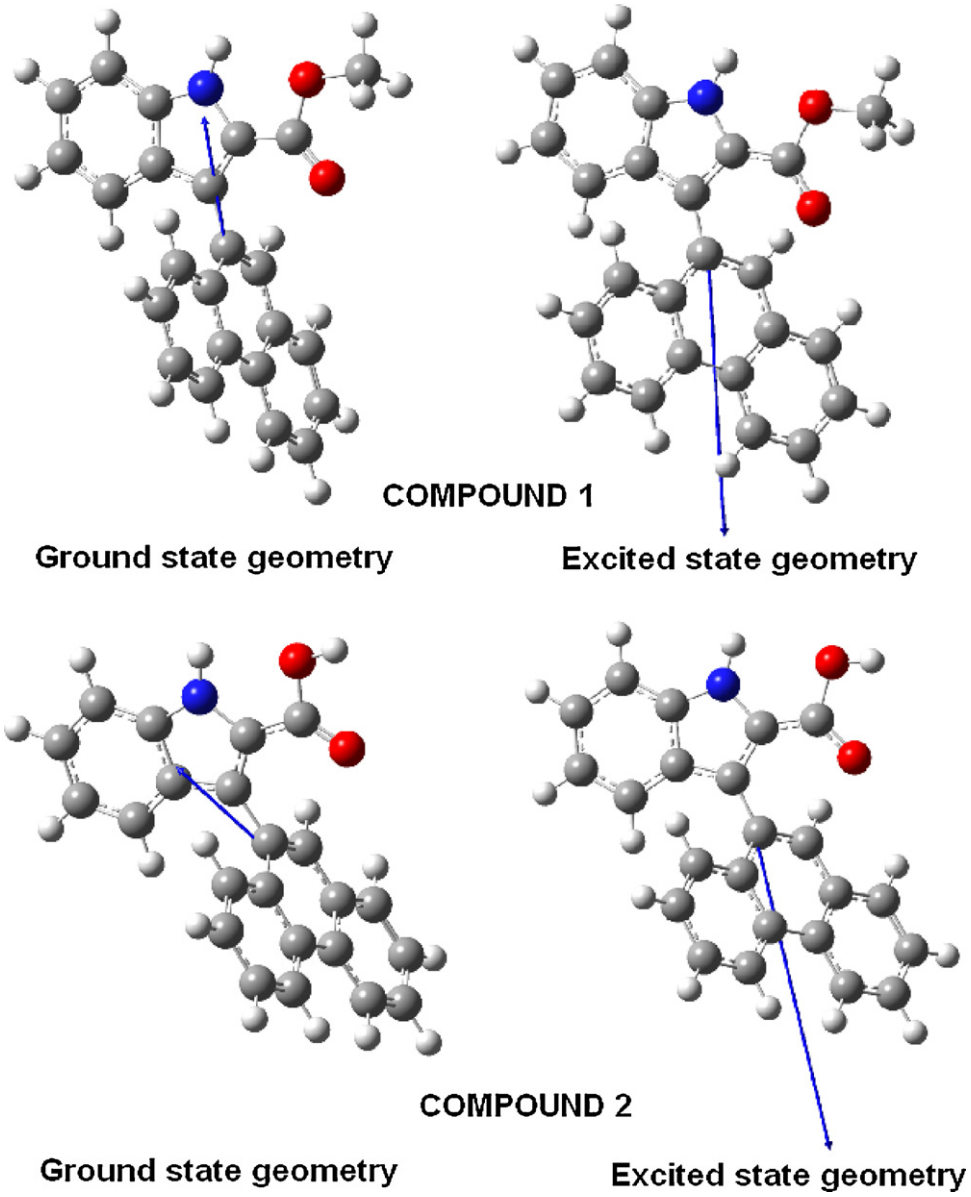

Fig. 5. Optimized geometries of compounds **1** and **2** obtained by Gaussian 09 software (grey: C atoms; white: H atoms; red: O atoms; blue: N atoms). Left: ground state; Right: lowest excited singlet state. The arrows indicate the direction of the dipole moment. (For interpretation of the references to colour in this figure legend, the reader is referred to the web version of the article.)

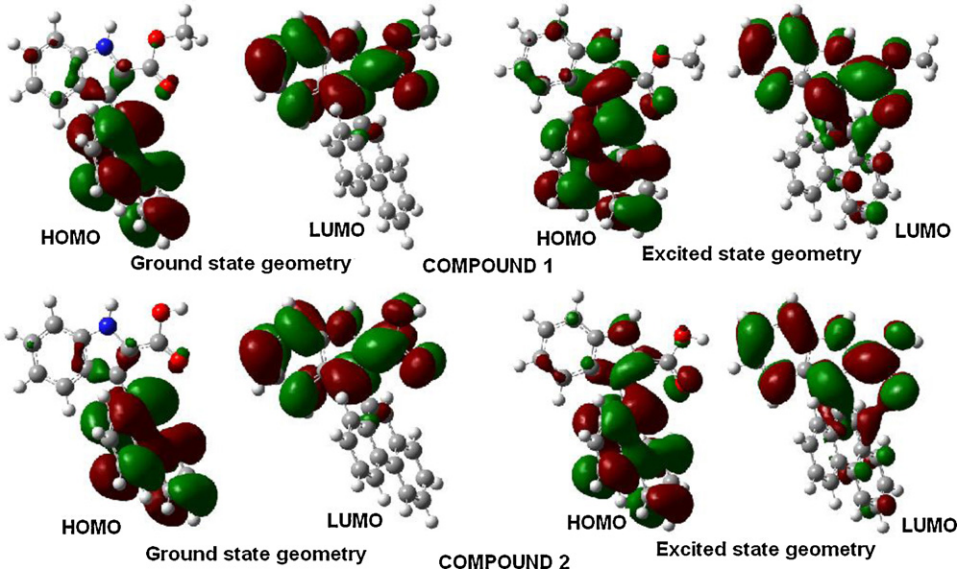

Fig. 6. Representation of HOMO and LUMO molecular orbitals of the phenanthrenyl-indoles **1** (above) and **2** (below). Left: optimized geometry for the ground state; Right: optimized geometry for the lowest excited singlet state.

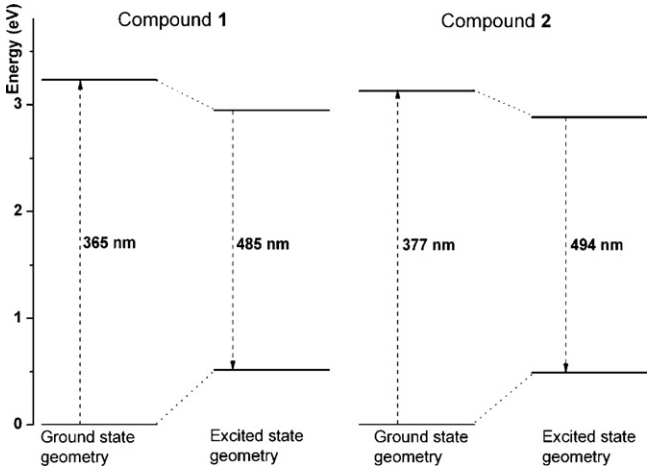

Fig. 7. Representation of the energy level diagram, with the transition energies for both compounds, obtained by molecular quantum chemistry calculations.

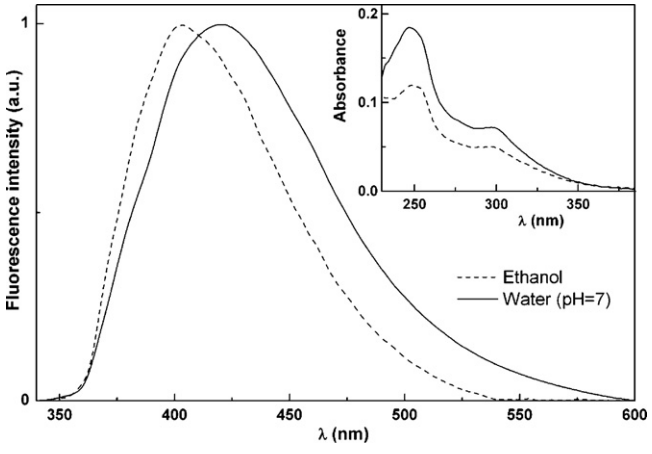

Fig. 8. Normalized fluorescence spectra (λ_{exc} = 325 nm) of 2×10^{-6} M solutions of peptide **3** in ethanol and aqueous buffer (pH = 7). Absorption spectra of 2×10^{-5} M solutions in the same solvents are shown as inset.

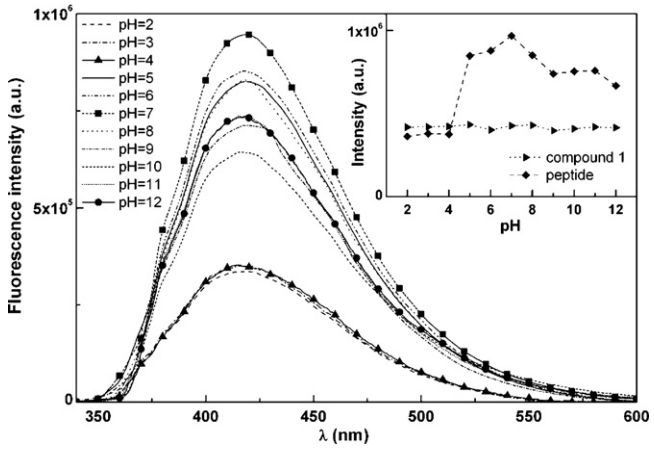

Fig. 9. Fluorescence emission spectra (λ_{exc} = 325 nm) of 1×10^{-6} M solutions of peptide **3** in aqueous media of variable pH. Inset: plots of emission intensity *vs.* pH for compound **1** alone (1×10^{-6} M) and linked to the peptide.

by the attachment of a Gly-Gly-Arg-Gly-Asp-Gly chain. The high flexibility and length of the peptide chain leads to the increase of the non-radiative decay pathways (in particular, due to additional vibrational modes) and consequent decrease of Φ_F values.

A fluorescence study with variable pH (2–12) was also performed, to evaluate the potential of compound **1** to serve as fluorescent pH probe alone or when inserted in peptides. It was found that compound **1** alone presents a fluorescence emission insensible to pH (inset of Fig. 9). However, when linked to the peptide chain, significant variations in the fluorescence intensity can be detected (Fig. 9). Changes in the maximum emission wavelengths are negligible. The rise in the fluorescence intensity (inset of Fig. 9)

Table 3
Maximum absorption (λ_{abs}) and emission wavelengths (λ_{em}), molar absorption coefficients (ε) and fluorescence quantum yields (Φ_F) for peptide **3**.

Solvent	λ_{abs} (nm) ($\varepsilon/10^4$ M^{-1} cm^{-1})	λ_{em} (nm)	Φ_F[a]
Ethanol	297 (0.25) 248 (0.60)	404	0.075
Aqueous buffer (pH = 7)	297 (0.36) 247 (0.92)	423	0.038[b]

[a] Relative to 9,10-diphenylanthracene in ethanol (Φ = 0.95 [19]).
[b] Non-deoxygenated solution.

Table 4
Steady-state fluorescence anisotropy (r) values and maximum emission wavelengths (λ_{em}) for compounds **1** and **2** and peptide **3** in mixed lipid membranes of DPPC/DPPG, below (25 °C) and above (55 °C) transition temperature of both lipids. Anisotropy values in glycerol at room temperature are also shown for comparison.

Lipid membrane composition	T (°C)	**1**		**2**		Peptide **3**	
		λ_{em} (nm)	r	λ_{em} (nm)	r	λ_{em} (nm)	$\bar{r}$
Neat	25	405	0.147	403	0.164	405	0.093
DPPC	55	407	0.061	405	0.089	405, 425 *sh*	0.064
DPPC/DPPG	25	406	0.131	405	0.145	405	0.078
3:1	55	408	0.061	407	0.078	406, 425 *sh*	0.050
DPPC/DPPG	25	409	0.127	407	0.124	406, 425 *sh*	0.076
1:1	55	410	0.056	409	0.073	407 *sh*, 425	0.043
DPPC/DPPG	25	411	0.109	411	0.120	408 *sh*, 420	0.071
1:3	55	410	0.045	413	0.062	408 *sh*, 420	0.040
Neat	25	414	0.087	415	0.107	412	0.063
DPPG	55	413	0.050	417	0.056	417	0.039
Glycerol	25	398	0.320	397	0.327	398	0.332

sh: shoulder.

starts at pH between 4 and 5. This variation can be related to the deprotonation of the side-chain carboxylic acid from the aspartic acid residue [34]. This could result in a hydrogen bond between the carboxylate anion and the indole group, affecting the peptide fluorescence quantum yield.

3.4. *Fluorescence of compounds **1**–**2** and peptide **3** in lipid membranes*

Photophysical studies of both compounds **1** and **2** and peptide **3** incorporated in lipid membranes composed of DPPC/DPPG mixtures were also performed. These two phospholipid molecules are the main components of biological membranes. It is known that, at room temperature, the neutral (zwitterionic) phospholipid DPPC (16:0 PC) and the anionic DPPG (16:0 PG) are in the ordered gel phase, where the hydrocarbon chains are fully extended and closely packed. Above the melting transition temperature, T_m = 41 °C [15] for DPPC and T_m = 39.6 °C [16] for DPPG, lipid chains attain the disordered and fluid liquid-crystalline phase.

The emission spectra of compounds **1** and **2** in lipid membranes of several DPPC/DPPG ratios at room temperature are displayed in Fig. 10. At 55 °C, the spectra in lipid membranes are very similar (data not shown) to those at lower temperature, with an expected fluorescence quenching (*ca.* 22% in neat DPPC and 45% in neat DPPG). In ethanol, the effect of increasing temperature (from 25 °C to 55 °C) in the fluorescence of these molecules is a ~42% reduction in intensity and a very small blue shift (1–2 nm for both compounds).

The fluorescence spectra in lipid membranes are similar for both compounds, displaying a red shift with increasing DPPG content in the lipid membrane (Fig. 10 and Table 4). As the difference between DPPC and DPPG molecules is only the polar head group, these results point to a higher hydration level of these compounds in DPPG rich vesicles. Another possibility for this behaviour is the occurrence of hydrogen bonding between the compounds and the OH groups of DPPG polar head.

Fluorescence anisotropy measurements (Eq. (4)) can give further information about these molecules behaviour in lipid membranes [35]. The fluorescence steady-state anisotropies determined for compounds **1** and **2** in lipid membranes of DPPC/DPPG are shown in Table 4. Anisotropy values in glycerol at room temperature were also determined for comparison, being similar for both molecules. The largest anisotropy values are observed in neat DPPC at gel phase (25 °C), that exhibits a melting transition temperature higher than DPPG.

The fluorescence anisotropy values (Table 4) clear indicate that both compounds are mainly located inside the lipid bilayers. At 25 °C (below the melting transition temperature of both lipids), the anisotropy of both molecules decreases monotonically with increasing DPPG content. The anisotropy values of both compounds are always higher in DPPC than in DPPG, the ratio r_{DPPC}/r_{DPPG} attaining *ca.* 1.5 times at 25 °C. Although DPPG molecules have a lower transition temperature, the difference between T_m values of DPPC and DPPG is only 1.4 °C. It is possible that some compound molecules are located in hydrated environments in DPPG,

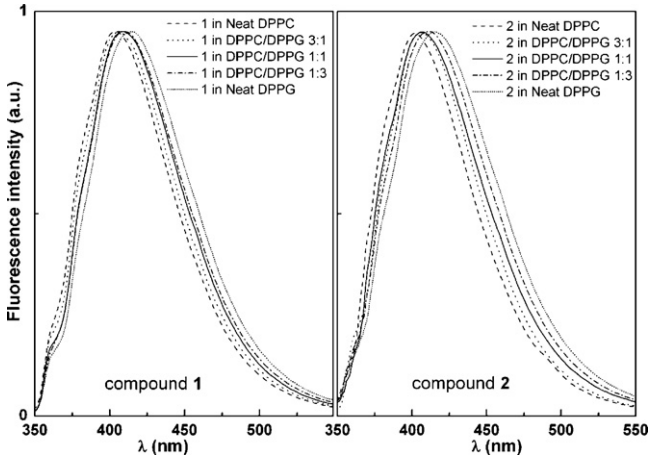

Fig. 10. Normalized fluorescence spectra of compounds **1** and **2** (2×10^{-6} M) in lipid membranes of DPPC/DPPG (λ_{exc} = 325 nm) at 25 °C.

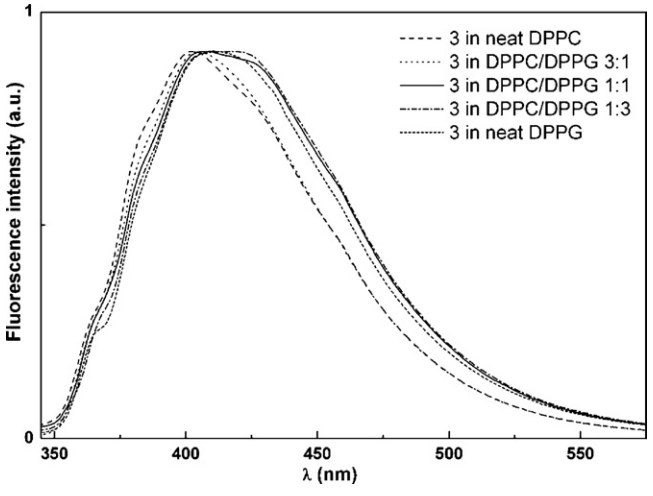

Fig. 11. Normalized fluorescence spectra of peptide **3** (2×10^{-6} M) in lipid membranes of DPPC/DPPG (λ_{exc} = 325 nm) at 25 °C.

Table 5
Steady-state fluorescence anisotropy (r) of the two anisotropy components, respective maximum emission wavelengths (λ_{max}) and weight of the first component (f_1) for peptide **3** in lipid membranes. Fluorescence quantum yields are also indicated.

Lipid membrane composition	T (°C)	f_1	r_1	$\lambda_{1,max}$ (nm)	r_2	$\lambda_{2,max}$ (nm)	Φ_F[a]
Neat DPPC	25	0.26	0.241	402	0.052	431	0.035
	55	0.31	0.142	402	0.033	432	0.013
DPPC/DPPG 3:1	25	0.10	0.242	402	0.063	422	0.031
	55	0.12	0.164	402	0.035	422	0.015
DPPC/DPPG 1:1	25	0.14	0.222	404	0.046	424	0.023
	55	0.16	0.133	404	0.023	431	0.012
DPPC/DPPG 1:3	25	0.11	0.191	402	0.066	421	0.030
	55	0.12	0.116	404	0.028	432	0.017
Neat DPPG	25	0.12	0.175	403	0.052	425	0.043
	55	0.20	0.089	405	0.028	435	0.020

[a] Relative to 9,10-diphenylanthracene in ethanol (Φ = 0.95 [19]).

near the polar head groups, justifying a further decrease in fluorescence anisotropy and the observed red shift in emission spectra. This behaviour is similar to that observed with a pyrenylindole-2-carboxylate [10b].

At 55 °C, when both phospholipids are at the liquid-crystalline phase, the anisotropy values of both compounds exhibit a significant reduction in all the lipid membranes, showing that these indolic derivatives clearly detect the phospholipid gel to liquid-crystalline phase transition.

Peptide **3** was also incorporated in the same lipid membranes. The emission spectra at 25 °C are presented in Fig. 11 (the spectra at 55 °C are similar in shape), and the fluorescence anisotropy values were also included in Table 4. Fluorescence spectra of **3** in lipid vesicles are clearly composed of two bands, one with maximum near 405 nm and another with maximum near 420 nm. Attaining to the spectra obtained in ethanol and in water (Fig. 8 and Table 3), these two bands can correspond to two different locations in liposomes, one in the lipid bilayer probably near the polar phospholipids head groups, and another in highly hydrated environments. The fluorescence anisotropy of the peptide in lipid membranes is also wavelength dependent and the r values presented in Table 4 are average values.

Due to this behaviour and considering the asymmetric nature of the peptide emission band (Fig. 8), the fluorescence anisotropy components (I_{VV} and $G{\cdot}I_{VH}$) were globally fitted to two sums of lognormal components (Eqs. (5) and (6)) [36], each sum characterized by a fitted anisotropy value, using a data analysis procedure previously developed by some of us [37],

$$I_{VV} = \sum_i \frac{A_{1i}}{(\lambda - (\lambda_{max})_{1i} + a_{1i})} \exp(-c_{1i}^2) \times \exp\left\{-\frac{1}{2c_{1i}^2}\left[\ln\left(\frac{\lambda - (\lambda_{max})_{1i} + a_{1i}}{b_{1i}}\right)\right]^2\right\} + \sum_i \frac{A_{2i}}{(\lambda - (\lambda_{max})_{2i} + a_{2i})} \exp(-c_{2i}^2) \times \exp\left\{-\frac{1}{2c_{2i}^2}\left[\ln\left(\frac{\lambda - (\lambda_{max})_{2i} + a_{2i}}{b_{2i}}\right)\right]^2\right\} \quad (5)$$

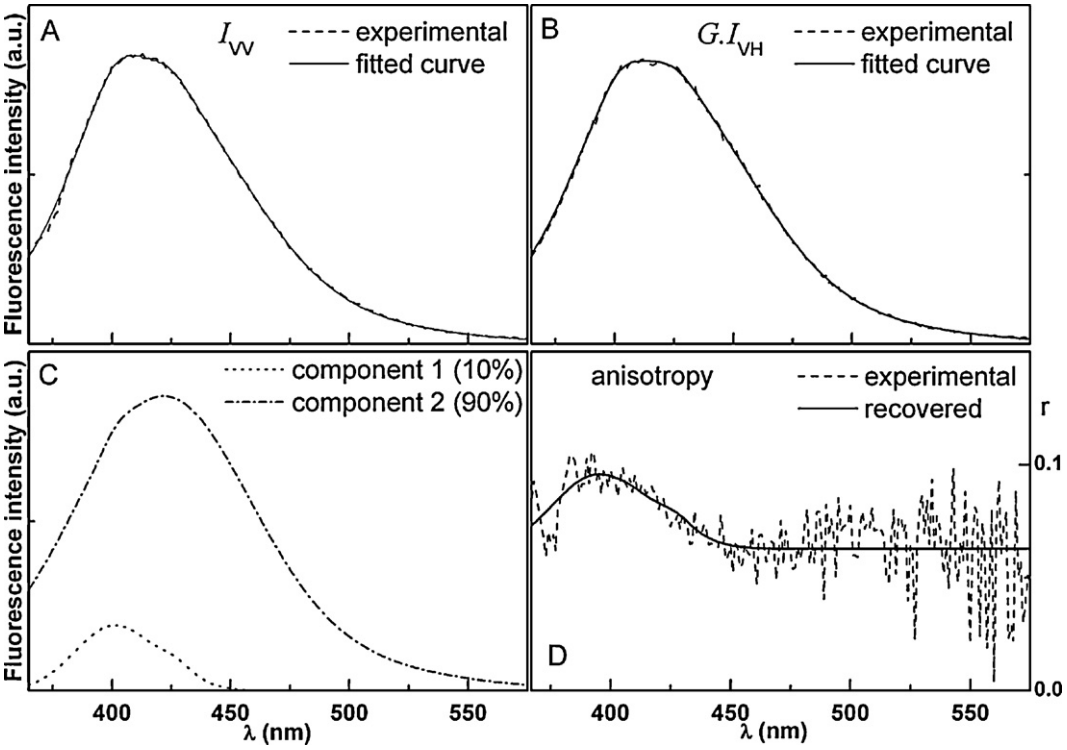

Fig. 12. Fit of peptide **3** emission in DPPC/DPPG 3:1 lipid membranes (25 °C). (A) I_{VV} component and fitted curve; (B) $G{\cdot}I_{VH}$ component and fitted curve; (C) recovered spectral components from the fitting procedure; (D) fluorescence steady-state anisotropy and recovered curve (calculated from the recovered components).

$$G \cdot I_{VH} = \sum_i \frac{A'_{1i}}{(\lambda - (\lambda_{max})_{1i} + a_{1i})} \exp(-c_{1i}^2) \times \exp\left\{ -\frac{1}{2c_{1i}^2} \left[\ln\left(\frac{\lambda - (\lambda_{max})_{1i} + a_{1i}}{b_{1i}} \right) \right]^2 \right\} + \sum_i \frac{A'_{2i}}{(\lambda - (\lambda_{max})_{2i} + a_{2i})} \exp(-c_{2i}^2) \times \exp\left\{ -\frac{1}{2c_{2i}^2} \left[\ln\left(\frac{\lambda - (\lambda_{max})_{2i} + a_{2i}}{b_{2i}} \right) \right]^2 \right\} \quad (6)$$

where A (or A') is the maximum intensity at wavelength λ_{max} and the parameters a, b and c are given by [36]

$$c = \frac{\ln(\rho)}{\sqrt{2\ln(2)}}, \quad b = H\frac{\rho}{\rho^2 - 1} \exp(c^2), \quad a = H\frac{\rho}{\rho^2 - 1} \quad (7)$$

where H is the half-width of the band and ρ is the skewness. The lognormal function sums account for the vibrational structure of compound spectrum. The components (1 and 2) have two different fitted anisotropy values, r_1 and r_2, given by

$$r_1 = \frac{A_{1i} - A'_{1i}}{A_{1i} + 2A'_{1i}} \quad \text{and} \quad r_2 = \frac{A_{2i} - A'_{2i}}{A_{2i} + 2A'_{2i}} \quad (8)$$

due to the additivity law of anisotropy [35],

$$r = \sum_i \frac{I_i}{I_{total}} r_i \quad (9)$$

with

$$r_i = \frac{(I_i)_{VV} - G(I_i)_{VH}}{(I_i)_{VV} + 2G(I_i)_{VH}} \quad (10)$$

Therefore,

$$A'_{1i} = A_{1i}\left(\frac{1 - r_1}{1 + 2r_1}\right) \quad \text{and} \quad A'_{2i} = A_{2i}\left(\frac{1 - r_2}{1 + 2r_2}\right) \quad (11)$$

Fig. 12 displays an example of the fit of anisotropy components, I_{VV} and $G{\cdot}I_{VH}$ (Eqs. (5) and (6)), and the fitting to the anisotropy curve, as well as the respective spectral contributions recovered from the fitting. The results are given in Table 5. In all cases, two components were recovered, one with higher anisotropy (r_1) and lower maximum emission wavelength ($\lambda_{1,max}$) and another with higher emission wavelength ($\lambda_{2,max}$) and very low anisotropy value (r_2).

Comparing the maximum wavelengths with the ones obtained for the emission in homogeneous solution (Fig. 8 and Table 3), it can be concluded that component 1 with λ_{max} = 402–405 nm corresponds to an environment similar to ethanol. This is the minor component (10–16%), attaining *ca.* 30% fraction in DPPC. The high anisotropy value, r_1, of this component points to a location inside the lipid bilayer, probably near the phospholipid polar head groups, feeling the transition to a more fluid phase at 55 °C, above T_m of both DPPC and DPPG. In general, the microviscosity of a lipid bilayer decreases from the interface to the interior of the membrane [38,39].

The major component, with maximum emission wavelength in the range 422–435 nm, corresponds to a hydrated environment, similar to pure water (Table 3). In fact, the anisotropy, r_2, is very low, pointing to a very fluid medium. Therefore, the RGD labelled peptide locates mainly in the outer part of the vesicle interfaces, in a medium with a fluidity approaching that of water. The fluorescence quantum yields of the peptide in lipid membranes (Table 5) are in accordance with this conclusion, as the values at room temperature are similar to the one measured in pure water (Table 3).

4. Conclusions

The 3-(phenanthren-9-yl)-1*H*-indole-2-carboxylic acid (**2**) obtained from the cleavage of the methyl ester of the methyl 3-(phenanthren-9-yl)-1*H*-indole-2-carboxylate (**1**) was inserted in solid phase into a peptide containing the RGD sequence. The peptide was also prepared by solid phase synthesis using a Fmoc strategy and 2-chlorotrityl chloride resin.

Both phenanthrenyl-indole derivatives **1** and **2** exhibit a solvent sensitive emission and generally high fluorescence quantum yields. The results point to the presence of a significant charge transfer mechanism in the excited state, especially for the compound with the carboxylic group.

Fluorescence measurements of the labelled peptide in solution showed a strong decrease in the fluorescence quantum yield, but a pH sensitive emission was detected.

The phenanthrenyl-indole derivatives and the labelled peptide were incorporated in lipid membranes of DPPC and/or DPPG. Steady-state fluorescence anisotropy measurements revealed that both indolic compounds are located inside the lipid bilayers and are able to report clearly the transition between the gel and liquid-crystalline phases. The RGD labelled peptide locates mainly in the outer part of the vesicle interfaces.

These results point to a promising utility of the phenanthrenyl-indole moiety as a fluorescence probe for biological systems, either as an extrinsic probe or as a label covalently bound to biomolecules.

Acknowledgements

Fundação para a Ciência e a Tecnologia (FCT)—Portugal, QREN and program FEDER/COMPETE for financial support through Centro de Física (CFUM) and Centro de Química (CQ-UM) of University of Minho and through the research project PTDC/QUI/81238/2006, co-financed by FCT and FEDER/COMPETE (FCOMP-01-0124-FEDER-007467). FCT is also acknowledged for grants BII of B.F.H., PhD of G.P. (SFRH/BD/38766/2007) and post-Doc. of A.S.A. (SFRH/BPD/24548/2005). The NMR spectrometer Bruker Avance III 400 is part of the Portuguese NMR Network (Rede/1517/RMN/2005) which is also supported by the FCT.

References

[1] J.B.A. Ross, A.G. Szabo, C.W.V. Hogue, Fluoresc. Spectrosc. 278 (1997) 151–190.
[2] S.M. Twine, A.G. Szabo, Methods Enzymol. 360 (2003) 104–127.
[3] A.R. Katritzky, T. Narindoshvili, Org. Biomol. Chem. 7 (2009) 627–634.
[4] E. Pazos, O. Vázquez, J.L. Mascarenas, M.E. Vázquez, Chem. Soc. Rev. 38 (2009) 3348–3349.
[5] R. Dayam, F. Aiello, J. Deng, Y. Wu, A. Garofalo, X. Chen, N. Neamati, J. Med. Chem. 49 (2006) 4526–4534.
[6] K.-E. Gottschalk, H. Kessler, Angew. Chem. Int. Ed. 41 (2002) 3767–3774.
[7] L.D. D'Andrea, A. Del Gatto, C. Pedone, E. Benedetti, Chem. Biol. Drug Des. 67 (2006) 115–126.
[8] E.A. Murphy, B.K. Majeti, L.A. Barnes, M. Makale, S. Weis, K. Lutu-Fuga, W. Wrasidlo, D. Cheresh, Proc. Natl. Acad. Sci. U.S.A. 105 (2008) 9343–9348.
[9] (a) E. Garanger, D. Botutyn, J.L. Coll, M. Favrot, P. Dumy, Org. Biomol. Chem. 4 (2006) 1958–1965;
(b) R.O. Hynes, Cell 69 (1992) 11–25;
(c) P.C. Brooks, R.A. Clark, D.A. Cheresh, Science 264 (1994) 569–571;
(d) R.O. Hynes, Nat. Med. 8 (2002) 918–921.
[10] (a) A.S. Abreu, E.M.S. Castanheira, P.M.T. Ferreira, L.S. Monteiro, G. Pereira, M.-J.R.P. Queiroz, Eur. J. Org. Chem. (2008) 5697–5703;
(b) G. Pereira, A.S. Abreu, E.M.S. Castanheira, P.J.G. Coutinho, P.M.T. Ferreira, M.-J.R.P. Queiroz, Eur. J. Org. Chem. (2009) 3906–3916;
(c) G. Pereira, E.M.S. Castanheira, P.M.T. Ferreira, M.-J.R.P. Queiroz, Eur. J. Org. Chem. (2010) 464–475.
[11] (a) A.S. Abreu, N.O. Silva, P.M.T. Ferreira, M.-J.R.P. Queiroz, Tetrahedron Lett. 44 (2003) 3377–3379;
(b) A.S. Abreu, N.O. Silva, P.M.T. Ferreira, M.-J.R.P. Queiroz, M. Venanzi, Eur. J. Org. Chem. (2003) 4792–4796.
[12] S. Batzri, E.D. Korn, Biochim. Biophys. Acta 298 (1973) 1015–1019.
[13] J.M.H. Kremer, M.W.J.v.d. Esker, C. Pathmamanoharan, P.H. Wiersema, Biochemistry 16 (1977) 3932–3935.

[14] J.R. Nordlund, C.F. Schmidt, S.N. Dicken, T.E. Thompson, Biochemistry 20 (1981) 3237–3241.
[15] B.R. Lentz, Chem. Phys. Lipids 50 (1989) 171–190.
[16] J.S. Vincent, S.D. Revak, C.D. Cochrane, I.W. Levin, Biochemistry 32 (1993) 8228–8238.
[17] J.N. Demas, G.A. Crosby, J. Phys. Chem. 75 (1971) 991–1024.
[18] S. Fery-Forgues, D. Lavabre, J. Chem. Educ. 76 (1999) 1260–1264.
[19] J.V. Morris, M.A. Mahaney, J.R. Huber, J. Phys. Chem. 80 (1976) 969–974.
[20] J.R. Lakowicz, Principles of Fluorescence Spectroscopy, Kluwer Academic/Plenum Press, New York, 1999.
[21] N. Mataga, T. Kubota, Molecular Interactions and Electronic Spectra, Marcel Dekker, New York, 1970.
[22] D. Creed, Photochem. Photobiol. 39 (1984) 537–562.
[23] B. Albinsson, M. Kubista, B. Nordén, E.W. Thulstrup, J. Phys. Chem. 93 (1989) 6646–6654.
[24] H. Lippert, H.-H. Ritze, I.V. Hertel, W. Radloff, Chem. Phys. Lett. 398 (2004) 526–531.
[25] I. Tatischeff, R. Klein, Photochem. Photobiol. 22 (1975) 221–229.
[26] N.J. Turro, Modern Molecular Photochemistry, Benjamin/Cummings Pub., Menlo Park (California), 1996.
[27] M.-J.R.P. Queiroz, A.S. Abreu, E.M.S. Castanheira, P.M.T. Ferreira, Tetrahedron 63 (2007) 2215–2222.
[28] M.-J.R.P. Queiroz, E.M.S. Castanheira, M.S.D. Carvalho, A.S. Abreu, P.M.T. Ferreira, H. Karadeniz, A. Erdem, Tetrahedron 64 (2008) 382–391.
[29] E.M.S. Castanheira, A.S. Abreu, M.S.D. Carvalho, M.-J.R.P. Queiroz, P.M.T. Ferreira, J. Fluoresc. 19 (2009) 501–509.
[30] D.R. Lide (Ed.), Handbook of Chemistry and Physics, 83th edition, CRC Press, Boca Raton, 2002.
[31] (a) K.C. James, P.R. Noyce, Spectrochim. Acta A 27 (1971) 691–696;
(b) G.R. Wileylb, S.I. Miller, J. Am. Chem. Soc. 94 (1972) 3287–3293.
[32] M.J. Frisch, G.W. Trucks, H.B. Schlegel, G.E. Scuseria, M.A. Robb, J.R. Cheeseman, G. Scalmani, V. Barone, B. Mennucci, G.A. Petersson, H. Nakatsuji, M. Caricato, X. Li, H.P. Hratchian, A.F. Izmaylov, J. Bloino, G. Zheng, J.L. Sonnenberg, M. Hada, M. Ehara, K. Toyota, R. Fukuda, J. Hasegawa, M. Ishida, T. Nakajima, Y. Honda, O. Kitao, H. Nakai, T. Vreven, J.A. Montgomery Jr., J.E. Peralta, F. Ogliaro, M. Bearpark, J.J. Heyd, E. Brothers, K.N. Kudin, V.N. Staroverov, R. Kobayashi, J. Normand, K. Raghavachari, A. Rendell, J.C. Burant, S.S. Iyengar, J. Tomasi, M. Cossi, N. Rega, J.M. Millam, M. Klene, J.E. Knox, J.B. Cross, V. Bakken, C. Adamo, J. Jaramillo, R. Gomperts, R.E. Stratmann, O. Yazyev, A.J. Austin, R. Cammi, C. Pomelli, J.W. Ochterski, R.L. Martin, K. Morokuma, V.G. Zakrzewski, G.A. Voth, P. Salvador, J.J. Dannenberg, S. Dapprich, A.D. Daniels, Ö. Farkas, J.B. Foresman, J.V. Ortiz, J. Cioslowski, D.J. Fox, Gaussian 09, Revision A.02, Gaussian, Inc., Wallingford, CT, 2009.
[33] F. Jensen, Introduction to Computational Chemistry, John Wiley & Sons, West Sussex, England, 1999.
[34] R.M.C. Dawson, D.C. Elliott, W.H. Elliott, K.M. Jones, Data for Biochemical Research, 3rd edition, Oxford University Press, 1989.
[35] B. Valeur, Molecular Fluorescence—Principles and Applications, Wiley-VCH, Weinheim, 2002.
[36] D.B. Siano, D.E. Metzler, J. Chem. Phys. 51 (1969) 1856–1861.
[37] E.M.S. Castanheira, M.S.D. Carvalho, D.J.G. Soares, P.J.G. Coutinho, R.C. Calhelha, M.-J.R.P. Queiroz, J. Fluoresc. (2010), doi:10.1007/s10895-010-0607-3.
[38] L. Tilley, K.R. Thulborn, W.H. Sawyer, J. Biol. Chem. 254 (1979) 2592–2594.
[39] M.A. Bahri, B.J. Heyne, P. Hans, A.E. Seret, A.A. Mouithys-Mickalad, M.D. Hoebeke, Biophys. Chem. 114 (2005) 53–61.